Enhanced mechanical heterogeneity of cell collectives due to temporal fluctuations in cell elasticity

Garrett Zills,[1] Trinanjan Datta,[1,2,*] and Abdul Naseer Malmi-Kakkada[1,†]
[1]*Department of Chemistry and Physics, Augusta University, 1120 15th Street, Augusta, Georgia 30912, USA*
[2]*Kavli Institute for Theoretical Physics, University of California, Santa Barbara, California 93106, USA*

(Received 25 March 2022; revised 16 September 2022; accepted 8 December 2022; published 6 January 2023)

Cells are dynamic systems characterized by temporal variations in biophysical properties such as stiffness and contractility. Recent studies show that the recruitment and release of actin filaments into and out of the cell cortex—a network of proteins underneath the cell membrane—leads to cell stiffening prior to division and softening immediately afterward. In three-dimensional (3D) cell collectives, it is unclear whether the stiffness change during division at the single-cell scale controls the spatial structure and dynamics at the multicellular scale. This is an important question to understand because cell stiffness variations impact cell spatial organization and cancer progression. Using a minimal 3D model incorporating cell birth, death, and cell-to-cell elastic and adhesive interactions, we investigate the effect of mechanical heterogeneity—variations in individual cell stiffnesses that make up the cell collective—on tumor spatial organization and cell dynamics. We discover that spatial mechanical heterogeneity characterized by a spheroid core composed of stiffer cells and softer cells in the periphery emerges within dense 3D cell collectives, which may be a general feature of multicellular tumor growth. We show that heightened spatial mechanical heterogeneity enhances single-cell dynamics and volumetric tumor growth driven by fluctuations in cell elasticity. Our results could have important implications in understanding how spatiotemporal variations in single-cell stiffness determine tumor growth and spread.

DOI: 10.1103/PhysRevE.107.014401

I. INTRODUCTION

Changes in cell biophysical properties play fundamental roles in cancer progression [1,2]. Biophysical techniques such as atomic force microscopy (AFM), optical trapping, and micropipette aspiration used to probe individual cell mechanical properties [3] show that cell stiffness grades the ability of tumor cells to metastasize, with softer cancer cells exhibiting the highest migratory and invasive potential [4]. Interestingly, while cancer tissues are generally stiffer than normal tissues, individual cancer cells themselves are softer than normal cells [4,5]. Given the impact of cell mechanics on cancer progression, insights into how mechanical heterogeneity—i.e., the idea that individual cells within a tumor can be characterized by different stiffnesses—emerge and consequently impact cell dynamics is important to understand. To address these questions, we used a minimal three-dimensional (3D) computational model of cell aggregates to show that time-dependent change in single-cell stiffness controls cell dynamics and mechanical heterogeneity of cell collectives.

Cell division, where a single cell divides into two, is a crucial process in the cell cycle marked by substantial changes in cell morphology, biochemistry, and mechanics [6,7]. Cell morphological change during division is driven by drastic remodeling of the cytoskeleton—a complex and dynamic network of proteins present in most animal cells [6,8–10]. The cell cortex is composed of a thin actin protein network bound to the cell membrane with a dense cross-linked meshwork architecture [11] that determines cell deformation in response to intercellular and extracellular forces [12]. Actin protein filaments that make up the cortex can dynamically polymerize and depolymerize leading to time-dependent variations in cell stiffness [13,14]. Recently, high temporal resolution AFM measurements of dividing embryonic cells showed that cell stiffness remarkably increased immediately prior to cell division and softened after cell division, exhibiting a periodic stiffening and softening [15]. Cell stiffness increased ∼threefold from ∼0.1 kilopascal (kPa) to ∼0.3 kPa prior to division and softened after division over a timescale of ∼20 min [15]. Such periodic stiffening and softening is directly driven by the accumulation of actin filaments in the cortical regions immediately prior to cell division and then redistribution into the cytoplasmic regions after division [15]. Similar mechanoadaptation is observed in tumor cells that soften to facilitate invasion in confined channels [16] and embryonic cells that soften to undergo collective cell migration [17].

Using a 3D computational model, we study the effect of rapid single-cell level stiffness change on the overall growth and dynamics of multicellular collectives. By varying the probability for cells to soften after division, we discover that mechanical heterogeneity, 3D cell dynamics and tumor growth are all enhanced due to time-dependent cell stiffness change. We reveal that cell division associated stiffening and softening determines the spatial structure and dynamics of 3D multicellular aggregates. Our results provide an explanation as to why softer cells which are directly correlated with heightened cancer progression and metastasis are

*Corresponding author: tdatta@augusta.edu
†Corresponding author: amalmikakkada@augusta.edu

preferentially located at the periphery of multicellular tumor spheroids as observed in experiments [2,4,18].

This article is organized as follows. In Sec. II we present the model and the method. In Sec. III we characterize the mechanical heterogeneity of tumor cell collectives and its impact on tumor cell dynamics. Finally, in Sec. V we present our conclusions.

II. MODEL AND METHOD

We utilized an agent-based simulation scheme for three-dimensional (3D) tumor growth to quantify how time-varying single-cell stiffness determines the spatial mechanical heterogeneity and dynamics of cells within a growing multicellular collective. Such off-lattice simulations are widely used in modeling tumor growth and recapitulate experimentally observed features of individual cell dynamics within cell collectives [19–25]. Agent-based models can simulate biophysical interactions between individual cells and provide insight into bridging the gap between single-cell and tissue-scale behaviors while capturing emergent cell collective behaviors [21,26,27]. Cell-cell interactions are typically modeled with short-ranged forces consisting of two terms: (1) elastic (repulsion) and (2) adhesive (attraction) forces. The magnitude of the elastic force (F_{ij}^{el}) between two cells i and j of radii R_i and R_j is given by [20,21]

$$F_{ij}^{el} = \frac{h_{ij}^{3/2}}{\frac{3}{4}\left(\frac{1-\nu_i^2}{E_i(t)} + \frac{1-\nu_j^2}{E_j(t)}\right)\sqrt{\frac{1}{R_i(t)} + \frac{1}{R_j(t)}}}, \tag{1}$$

where ν_i and E_i are the Poisson ratio and elastic modulus of the ith cell. Here h_{ij} is the overlap (virtual) distance between the two cells. The time-varying cell elastic modulus, $E_i(t)$, which we refer to as the cell stiffness is the key parameter that we focus on in this study. Prior works have considered the cell stiffness to be *time independent* [19–21,23–25]. The adhesive force F_{ij}^{ad} between cells is

$$F_{ij}^{ad} = A_{ij} f^{ad} \tfrac{1}{2}\left(c_i^{\rm rec} c_j^{\rm lig} + c_i^{\rm lig} c_j^{\rm rec}\right), \tag{2}$$

where A_{ij} is the overlap area between the two cells in contact and f^{ad} determines the strength of adhesive bond [20,21]. The receptor (rec) and ligand (lig) concentrations (c) are normalized by the maximum receptor and ligand concentrations to satisfy $c_i^{\rm rec} = \bar{c}_i^{\rm rec}/c^{\rm rec,max} = 0.9$ and $c_i^{\rm lig} = \bar{c}_i^{\rm lig}/c^{\rm lig,max} = 0.9$. The adhesion coefficient f^{ad} can always be rescaled by absorbing the maximum possible values of the receptor and ligand concentrations: $c^{\rm rec,max}$ and $c^{\rm lig,max}$, respectively. Our prior work showed that the values of f^{ad} and the receptor-ligand concentration we consider are consistent with experimental measurements of cell-cell adhesion strength [22] but is not a general constraint.

Starting with 100 cells randomly placed in a 3D cubic volume, we simulate tumor cell collective growth over ∼7.5 days, sufficient to account for multiple cell division cycles. As cells grow, divide, and move the multicellular collective grows into a large spheroid with cells in the core and periphery, mimicking the growth of tumor spheroids [28] and organoids [18] as observed in experiments. The effect of forces that cells experience from its microenvironment on growth is accounted through the pressure, p_i, that cells feel due to neighboring cells using the minimal definition [19–21],

$$p_i = \sum_{j=1}^{NN(i)} \frac{|F_{ij}|}{A_{ij}}. \tag{3}$$

Here the sum is over the nearest neighbors (NN) of the ith cell and $|\cdots|$ denotes the absolute value. The cell nearest neighbors are defined by calculating the overlap between two cells $h_{ij} = \max[0, R_i + R_j - |\mathbf{r}_i - \mathbf{r}_j|]$ where R_i, R_j are cell radii and $\mathbf{r}_i - \mathbf{r}_j$ is the center-to-center distance between cells i, j. $h_{ij} > 0$ selects cells that are in contact with any given cell. If p_i is smaller than a predetermined threshold value, p_c, cells grow in size and divide. However, if $p_i > p_c$, the cell becomes dormant which stalls size growth and division. We set $p_c = 0.1$ kPa on the basis of our prior work where we quantitatively reproduced experimental data for time-dependent tumor growth under externally applied pressure [21]. A cell can switch between dormancy and growth depending on whether the ratio of $\frac{p_i(t)}{p_c}$ is greater than or less than 1 [22]. The volume of an individual cell grows in time at a mean rate,

$$r_V = \frac{2\pi (R_m)^3}{3\tau}, \tag{4}$$

and divides into two cells upon reaching a critical radius $R_m = 5$ μm. On division, the parent cell and the newly created daughter cell take on radii $R_d = \frac{R_m}{2^{\frac{1}{3}}}$ to ensure volume conservation. Hence, a key timescale in the simulation is τ, the average time it takes for a cell to divide, set to be ∼15 hr, comparable to typical cell division times [20,29]. We incorporate cell death in the simulations by randomly removing particles at a rate $k_d = 10^{-6}$ s^{-1}. Owing to the death rate being much smaller than the birth rate ($k_d \ll \frac{1}{\tau}$), we are simulating a rapidly expanding collection of cells.

In this article we restrict ourselves to a minimal computational model where we do not consider important cell features such as actomyosin-mediated contractility. Even though we simplified many of the complexities associated with cell behaviors, our results point out that cell stiffening prior to division and softening after division driven by the recruitment and release of actin filaments from the cell cortex has important consequences on the dynamics and spatial organization of multicellular collectives.

A. Time variation in single-cell stiffness

To investigate whether temporal variation in single-cell stiffness affects 3D cell collective spatial organization and dynamics, we coupled cell division to cell stiffness change according to two simple rules: (1) First, as the size of a cell approaches the mitotic radius, at $R_i(t = t^*)/R_m = 0.98$, its stiffness is increased to $E_i(t > t^*) = \min\{2.5 \times E_i(t^*), 3\ \text{kPa}\}$ i.e., minimum of the value between 2.5 times the cell stiffness at time t^* and a maximum stiffness value of 3 kPa. This ensures that the maximum cell stiffness is 3 kPa and prevents it from increasing to unphysical values. Tumor cells tend to be stiffer than embryonic cells and the stiffness range we consider have been experimentally reported [16]. The condition $R_i(t = t^*) = 0.98 \times R_m$ is set to ensure that stiffness change occur immediately before cell division

TABLE I. The parameters used in the simulation. The parameters where we indicate the mean and standard deviation are sampled from a normal distribution. For details, see [21].

Parameters	Values
Timestep (Δt)	10 s
Critical radius for division (R_m)	5 μm
Environment viscosity (η)	0.005 kg/(μm s)
Average division time (τ)	54 000 s
Adhesive coefficient (f^{ad})	1×10^{-4} μN/μm^2
Initial mean elastic modulus (E_i) (standard deviation)	1 kPa (0.1 kPa)
Mean Poisson ratio (ν_i) (standard deviation)	0.5 (0.02)
Death rate (k_d)	10^{-6} s^{-1}
Mean receptor concentration (c^{rec}) (standard deviation)	0.9 (0.02) [normalized]
Mean ligand concentration (c^{lig}) (standard deviation)	0.9 (0.02) [normalized]
Threshold pressure (p_c)	10^{-1} kPa

at $R = R_m$. (2) Second, to mimic experimentally observed cell softening after division, we implement a probabilistic protocol for cell softening:

(1) Draw a uniformly distributed random number, u, in the interval (0,1)

(2) If u is less than or equal to the softening probability parameter χ, reduce cell stiffness to $E_i(t > t') = \max\{0.2 \times E_i(t'), 0.5\ \mathrm{kPa}\}$. If $u > \chi$, the parent cell does not soften. χ is an input parameter that we vary in the model.

To prevent cell stiffness from approaching zero, we implement a lower bound of cell stiffness at 0.5 kPa. The initial condition for daughter cell mean stiffness is set to 1 kPa and characterized by a Gaussian distribution with standard deviation of 0.1 kPa (see Table I). The range of stiffness values between 0.5–3 kPa we consider is in the physiological range for cell stiffnesses [30] with the lower and upper end corresponding to embryo cell stiffness and lung cell stiffness, respectively [31]. We chose the radius at which a cell undergoes stiffening prior to division as $R_i(t = t)/R_m = 0.98$ so as to model the experimental scenario where cells start stiffening ∼20 min prior to division. For the mean cell cycle time of $\tau =$ 54 000 s, the time interval between cell stiffening and reaching the mitotic radius R_m when a cell divides is given by $t_{\mathrm{int}} \sim (1 - 0.98) \times 54\,000$ s $\sim$ 20 min. The schematic of single-cell stiffness change is visualized in Fig. 1(a). The time-dependent single-cell stiffness change obtained in the simulation for selected cells at three different χ values are shown in Fig. 1(b). At $\chi = 1$ intermittent cell stiffening and softening events are visible [bottom panel, Fig. 1(b)] compared to $\chi = 0$ whereby cells do not soften [top panel, Fig. 1(b)].

We now describe the molecular underpinnings of the cell stiffness change implemented in the computational model. As cells progress through the cell cycle and approach division, actin filaments accumulate at the boundary of the cell, increasing cell stiffness. After division, the acto-myosin filaments are distributed into the cytoplasmic regions of the cell until the cell is ready for the next division event [15,32,33]. The probability for the cortical protein filaments to be redistributed into the cytoplasm is modeled in our simulation via the parameter χ, which we vary from 0 to 1, at intervals of 0.1. Hence, $\chi = 0.1$ implies a very low probability for cells to soften, while $\chi = 1$ implies a high probability for cells to soften after division. We note that the parent cell stiffness is dynamically increased before division. After division, the daughter cell stiffness is set from the initial condition as noted in Table I while the parent cell undergoes softening as determined by the parameter χ. When the daughter cell grows in size and approaches the mitotic radius as noted above $[R_i(t = t^*)/R_m = 0.98]$, they can undergo stiffening followed by softening. Furthermore, some cells may become dormant after stiffening and not progress to division depending on the pressure parameter. This would lead to the arrest of single-cell stiffnesses at heightened values irrespective of χ. The overall change in average cell stiffness of the cell collective as a function of time is shown in Fig. 1(c). At $\chi = 1$, the cell collective is on average softer as opposed to a stiffer cell collective at $\chi = 0$. Based on varying the parameter χ we can now study the impact of cell division associated cell softening and stiffening on cell dynamics within the 3D cell collective.

To check the robustness of our results, we implement a gradual increase in cell stiffness over a ∼20 min time interval as discussed in Appendix C. Furthermore, we varied the radius at which cell is stiffened prior to division over a range of $R_i(t = t^*)/R_m$ values as discussed in Appendix D.

B. Cell dynamics

In addition to the active forces due to cell growth and division, the passive forces experienced by a cell due to interaction with its neighbors contributes to cell dynamics. The net force $\mathbf{F}_i$ on the ith cell is the vectorial sum of elastic and adhesive forces that the neighboring cells exert on it, $\mathbf{F}_i = \sum_{j=1}^{NN(i)} \mathbf{F}_{ij}$. Here j is summed over the number of nearest neighbors $NN(i)$. We performed over damped (low Reynolds number [34]) dynamics without thermal noise because the viscosity of the medium surrounding cells is assumed to be large [21]. In the context of a growing tumor spheroid, the expansion of the tumor front driven by proliferation will overtake cell movement due to random displacements allowing us to neglect additional stochastic forces [20,21]. Therefore, the equation of motion for a cell is

$$\dot{\mathbf{r}}_i = \frac{\mathbf{F}_i}{\gamma_i}, \tag{5}$$

where $\gamma_i = 6\pi\eta R_i$ is the friction term which models the environment as a thick gel. At least 12 simulations each for 10 different values of the cell softening parameter χ were conducted to study its impact on cell dynamics, size of the cell collective, and spatial mechanical heterogeneity. The various parameters utilized in the computational model are summarized in Table I.

There are two timescales that are important in our computational model: (1) elastic cell-cell interaction timescale $\tau_{el} \sim \frac{\gamma}{ER}$ of $O(100\ \mathrm{s})$ and (2) the timescale τ associated with the cell division of $O(50\,000\ \mathrm{s})$. As we are interested in the long-time dynamics of the cell collective at timescales greater than τ, we consider the time taken for the cell to stiffen and

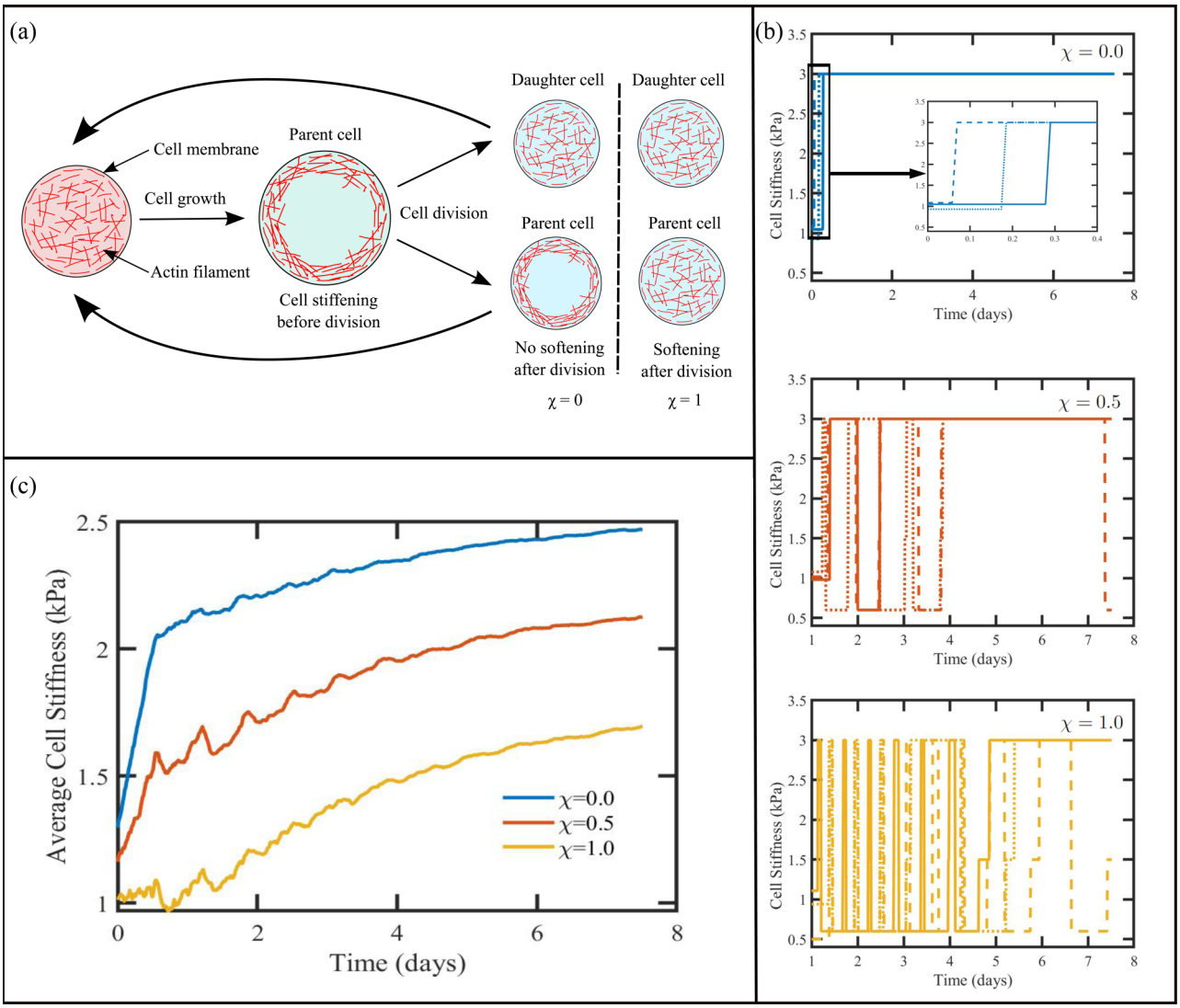

FIG. 1. 3D tumor growth model with time-varying single-cell stiffness. (a) Schematic illustrating time-varying single-cell stiffness change implemented in the simulation. The cell stiffness increases prior to division due to the accumulation of actin filaments (red lines) at the cell cortex and soften immediately after division due to the release of cortical actin into the cell cytoplasm, as controlled by the parameter for cell softening probability χ. $\chi = 0$ implies no softening of the parent cell, while $\chi = 1$ leads to both parent and daughter cell softening after division. The daughter cell stiffness after division is set from a fixed initial condition. (b) (Top panel) Time-dependent individual cell stiffness change at $\chi = 0$. Multiple lines are for selected individual cells from the simulation. Inset shows a zoom into the region where cell stiffness increases. (Middle panel) Cell stiffness vs time at $\chi = 0.5$ and (bottom panel) at $\chi = 1$. (c) Average cell stiffness in the 3D cell collective as a function of time at three different values of $\chi = 0, 0.5, 1$.

soften to occur instantaneously given that it is a fast process compared to cell division. We note that the growing spheroid that we consider is a nonequilibrium system [21,23,35].

III. RESULTS

While the molecular factors that determine tumor growth are better understood, much remains to be known about the impact of time-dependent changes in cell physical properties on the spatial mechanical heterogeneity of 3D cell collectives. Given that individual cells that make up a tumor are characterized by broadly varying stiffnesses we wondered whether cell subpopulations, i.e., clusters of cells with differing levels of stiffness are spatially organized within cell collectives. To answer this question we visualized the multicellular spheroids generated from our simulations at $t = 12\tau$ and $\chi = 1$ [Fig. 2(a)]. A mixture of soft (lighter color) and stiff (darker color) cells are visible on the surface of the spheroid. As we are interested in understanding the spatial variation in cell stiffness, a cross-sectional view with respect to a 2D plane cutting through the center of the 3D cell collective is shown in Fig. 2(b). Remarkably, a clear trend in spatial mechanical heterogeneity with stiffer cells in the core and softer cells at the periphery is visible. To quantify this further, we grouped cells according to their positions with respect to the tumor center of mass, $\mathbf{R}_{CM} = \frac{1}{N}\Sigma_i^N \mathbf{r}_i$, where N is the total number of cells. By calculating the cell distances from the tumor center of mass, $d_i = |\mathbf{r}_i - \mathbf{R}_{CM}|$, where $|\cdots|$ indicates vector magnitude we group cells into eight cell subpopulations. Cells closest to the center of mass compose the core of

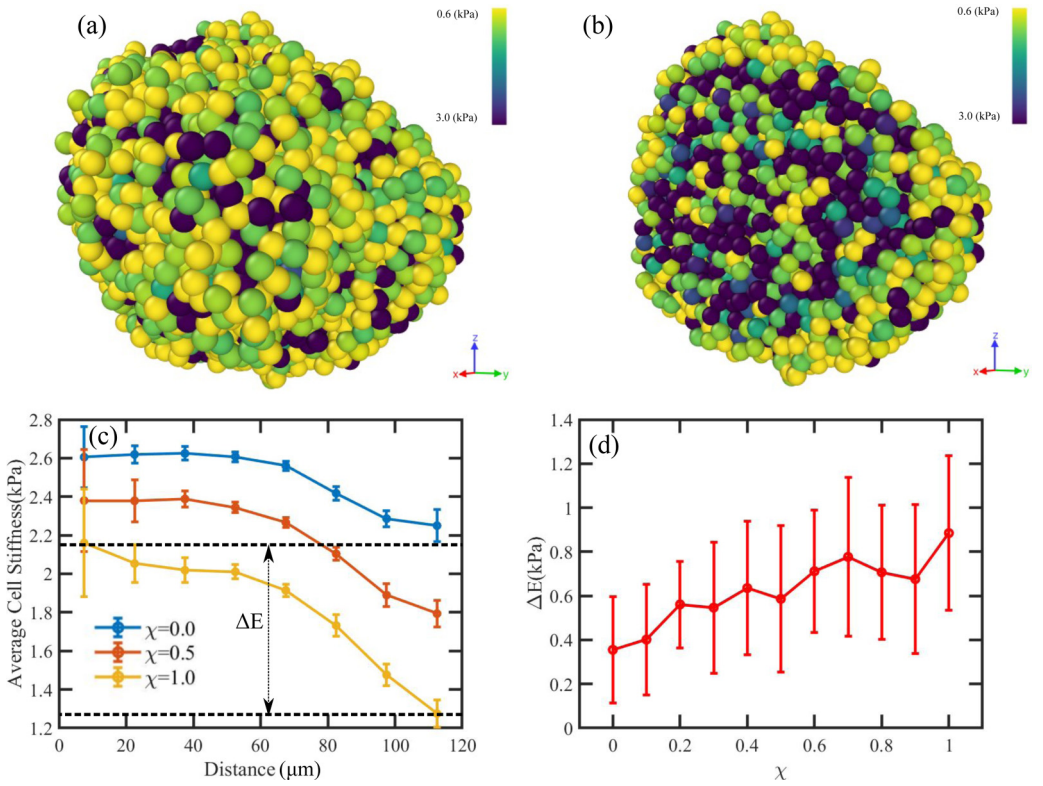

FIG. 2. Spatial heterogeneity in cell subpopulation stiffness between core and periphery in growing 3D cell collectives. (a) Snapshot of the 3D collection of ∼6000 cells at $t = 7.5$ days for $\chi = 1$. Each small sphere is a single cell of maximum diameter 10 μm with the color visualizing cell stiffness (see color bar). (b) Cross section through one plane of the 3D cell collective showing the core and periphery. Stiffer cells (darker color) are visible at the core with softer cells at the periphery. (c) Average stiffness of cell subpopulations as a function of distance from the core. Cell subpopulations are categorized according to their distances from the center of mass of the 3D cell collective. Circles indicate mean values, and the error bar is the standard deviation. A marked difference between cell subpopulation stiffness at the core vs periphery is noted at $\chi = 1$, as quantified by ΔE. (d) Mechanical heterogeneity of the cell subpopulation stiffness is quantified using ΔE. Difference in the average cell stiffness between the core and periphery is most pronounced at $\chi = 1$.

the spheroid and we refer to the outermost subpopulation as the periphery.

The thickness of each layer composing the cell subpopulation is set to 15 μm. The statistical average of single-cell stiffnesses, E_i, within each subpopulation is computed at time $t = 12\tau$ using

$$\langle E(r_d)\rangle = \frac{\Sigma_i E_i \delta(r_d - d_i)}{\Sigma_i \delta(r_d - d_i)}, \tag{6}$$

where r_d is the binning distance from the tumor center of width 15 μm and $\delta(r_d - d_i) = 1$ if d_i is within the distance range r_d and 0 otherwise.

Notably, cells located near the core of the tumor spheroid are stiffer as compared to cells near the periphery [Fig. 2(c)], irrespective of the value of χ. As expected, the overall cell subpopulation is stiffer at low χ which corresponds to low probability for cells to soften after division. We discover that the stiffness heterogeneity between cell subpopulations in the core and periphery increases with χ. To quantify the spatial mechanical heterogeneity between cell subpopulations, we calculated the difference in average stiffness between the core and periphery,

$$\Delta E = \langle E\rangle_{\text{core}} - \langle E\rangle_{\text{periphery}} \tag{7}$$

[see Fig. 2(d)]. At $\chi = 0$, the spatial mechanical heterogeneity is low with a mean $\Delta E \sim 0.35$ kPa as compared to $\Delta E \sim 0.8$ kPa at $\chi = 1$. The spatial mechanical heterogeneity is therefore enhanced at $\chi = 1$, indicating that time-varying cell stiffness change during cell division is an important determinant of mechanical heterogeneity. As mechanical heterogeneity during cancer progression is thought to facilitate metastasis [2,30,36], spatial heterogeneity of tumor organoids with a stiffer core and softer periphery of cells may be a general feature of 3D tumor cell collectives [18].

With a view of providing an intuitive argument as to how the mechanical heterogeneity emerges, we conducted additional analysis of our results. We anticipate that cells in the core may experience extra pressure which would limit cell division and lead to stiffer cells. On the other hand, with lower pressure in the periphery, cells can easily divide leading to softer cells. Hence, we first analyzed the average pressure vs distance from the core to the periphery of the multicellular spheroid. As expected, pressure in the core is elevated [see Fig. 3(a)] which should limit cell division events. Pressure is significantly lower as one approaches the periphery indicating that division events will be enhanced at the periphery as compared to the core. To confirm that pressure does indeed have the anticipated effect on the number of cell division events, we calculated the growth rate as a function of distance

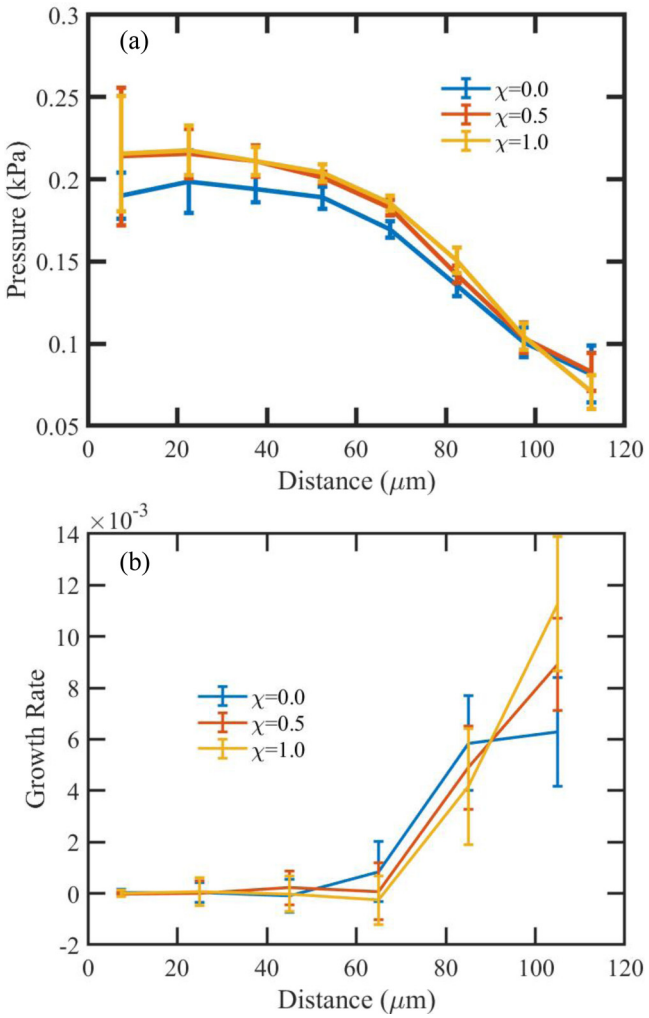

FIG. 3. (a) Average pressure vs distance from the core. High pressure at the core and lower pressure at the periphery is observed independent of the value of χ. Higher pressure is expected to restrict division events at the core leading to stiffer cells. On the other hand, division events at the periphery lead to softer cells. (b) Growth rate which quantifies the ability of cells to divide shows that there are no cell division events within the core and heightened cell divisions at the periphery. Growth rate is notably higher when there is a greater tendency of parent cell to soften after division ($\chi = 1$).

[see Fig. 3(b)] using

$$\Gamma(r) = \frac{N(r,t) - N(r,t-\delta t)}{\delta t}, \tag{8}$$

where $N(r,t)$ is the number of cells at time $t = 12\tau_{\min}$ and $\delta t \simeq 0.1\tau_{\min}$. As anticipated, the growth rate $\Gamma(r)$ is dependent on the distance r from the core of the multicellular spheroid. The spatial profile for the number of cell divisions is in agreement with our results for the spatial trend in pressure experienced by cells with low number of divisions in the core and enhanced cell divisions at the periphery. This allows us to conclude that extra pressure in the core limits cell division and prevents cell softening. On the other hand, prolific cell division events in the periphery results in softer cells at the periphery, leading to the mechanical heterogeneity in the cell stiffness that we observe.

The pressure experienced by cells is self-generated as a consequence of cell growth and division. Pressure is a highly variable quantity characterized by a broad distribution which changes with time [21,22]. Hence, even though a large change in pressure is not noted due to varying softening probability, marked differences in the growth rate are visible in Fig. 3(b). Additionally, pressure is measured at a single time point while the growth rate is measured over a finite time interval.

Next we investigated whether the dynamics of individual cells that make up the spheroid could be affected by the spatial mechanical heterogeneity. Prior studies report that metastatic tumor cells are softer compared to nonmetastatic tumor cells [18,37–40]. As cell division events fluidize cell collectives and lead to superdiffusive dynamics [21,23], division-dependent cell softening could affect the nonequilibrium active forces that cells experience and thus affect individual 3D cell dynamics. By tracking single-cell trajectories, we calculate both single-cell mean-squared displacement (scMSD) and ensemble-averaged MSD,

$$\Delta(t) = \left\langle \frac{1}{N'} \Sigma_{i=1}^{N'} [\mathbf{r}_i(t) - \mathbf{r}_i(0)]^2 \right\rangle, \tag{9}$$

where N' denotes the total number of tracked cells from the beginning to the end of the simulation. The ensemble average $\langle \cdots \rangle$ is over 12 different simulation runs at each value of χ for different initial conditions (see Appendix A). scMSD (without averaging over N' or multiple simulation runs) shown in Fig. 4(a) reveal that distances traversed by cells are highly heterogenous. While majority of the cells traverse distances less than $\sqrt{500\ \mu\text{m}^2} = 22.4\ \mu\text{m}$, a population of highly dynamic cells exist that traverse distances on the order of $\sqrt{3000\ \mu\text{m}^2} = 54.7\ \mu\text{m}$ [Fig. 4(a)] at $\chi = 1$. Another interesting feature is the intermittent change in scMSD clearly visible in the highly dynamic group of cells where there are steep increases in scMSD followed by time regimes where scMSD does not change much.

As cell collectives exhibit glass to fluid-like transition due to cell division events [21,41,42], we surmise that cell displacement could be linked to cell division events and the associated time-dependent change in stiffness. Hence, we investigate the effect of cell softening probability on ensemble-averaged MSD [Fig. 4(b)]. At short times, $t < 2$ days, probability of cell softening (χ) has no visible effect on the cell dynamics as observed from the MSD plots. In contrast, at longer times $t > 2$ days, cell dynamics is significantly restricted at low χ. As the MSD is significantly enhanced at $\chi = 1$, we confirm that higher χ values resulting in enhanced spatial mechanical heterogeneity with larger stiffness asymmetry between cells in the core and the periphery [see Fig. 2(d)] is more conducive to 3D cell dynamics. To confirm that the space explored by cells increase with χ, we analyze the maximum (max) MSD at $t = 12\tau$ during each individual simulation run [see stars in the inset of Fig. 4(b)]. The max MSD at multiple χ values are summarized in Fig. 4(c), which increases with χ. Therefore, on the basis of the spatial mechanical heterogeneity we report in Fig. 2, a stiffer core and softer peripheral cells is conducive to heightened cell dynamics as indicated by the larger MSD values.

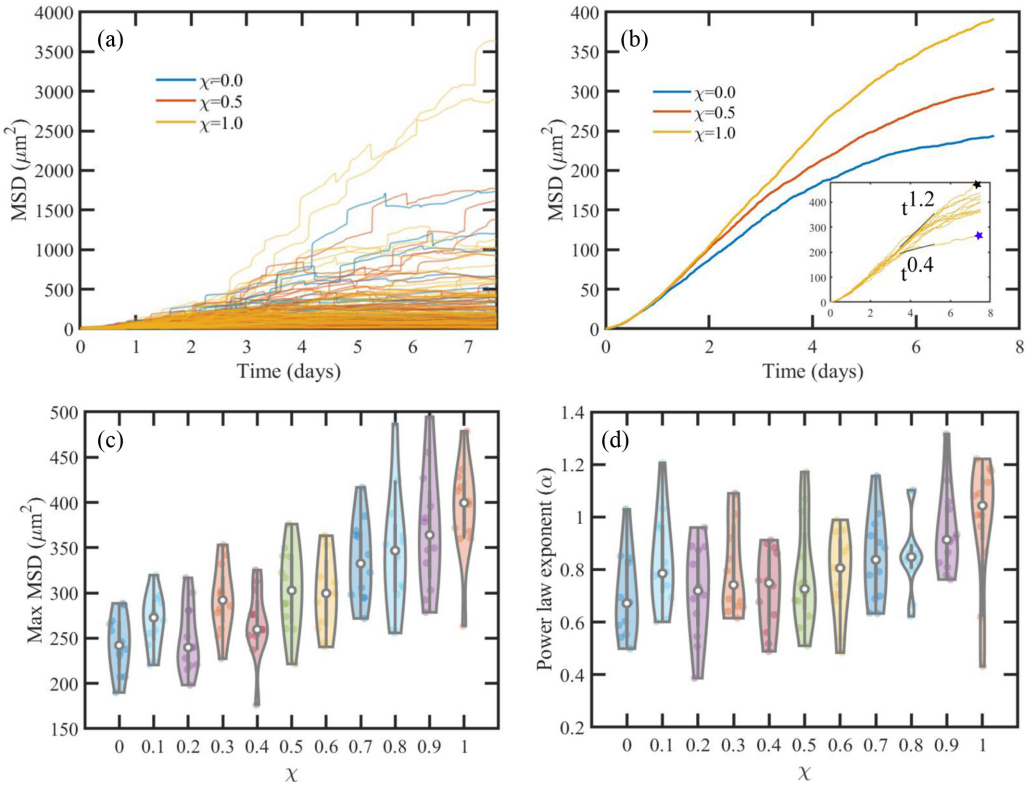

FIG. 4. Cell softening after division leads to distinct cell dynamic behaviors. (a) Single-cell MSD (scMSD) vs time, at $\chi = 0$ (blue), $\chi = 0.5$ (red), and $\chi = 1$ (yellow). ∼60 scMSDs per χ value show highly heterogenous dynamics with some cells traversing large distances, while other cells move less in comparison to the typical cell diameter of 10 μm. (b) Ensemble-averaged MSD of cells vs time at three different values of χ. The data are averaged over 12 independent simulation runs by tracking ∼800 cells over the complete simulation at each value of χ. Inset: MSD from averaging over cells from individual simulation runs at $\chi = 1$. The maximum (max) MSD value for two individual simulation runs are marked with stars. The time regime where MSD is fit to power law in order to extract the MSD exponent is shown. (c) Max MSD increases as a function of χ. Colored dots represent each of the Max MSD values from individual simulation runs. White dots are the median values and the thick line within the violin distribution represent the interquartile range between the first and third quartiles. The bottom and top edge of thinner gray lines mark the lower and upper adjacent values respectively. (d) By fitting cell-averaged MSD in each of the 12 simulation runs to a power law, we extracted the MSD exponent (α) as a function of χ. Cell dynamics is significantly enhanced at $\chi = 1$ as compared to $\chi = 0$. Note: the envelope in the violin plots indicate the frequency at which y axis values occur. The wider the violin plot the greater the frequency of those values. The lateral displacement of points are for visualization purposes only.

MSD is known to depend on the mechanical resistance of the surrounding medium [43], but the influence of individual cell level change in mechanical properties such as stiffness on MSD is unclear. Time-dependent scaling of MSD based on a fit to power law $\Delta(t) \sim t^{\alpha}$ reveals important features of cell dynamics [see black lines in the inset of Fig. 4(b) for details]. When $\alpha = 1$, cells exhibit diffusive random walk. For cells undergoing directed motion, the power-law exponent is greater than one ($\alpha > 1$) in contrast to restricted cell motion which leads to a sublinear rise in MSD with $\alpha < 1$. Interestingly, median α values show that cells exhibit subdiffusive motion due to time-varying stiffness change except at $\chi = 1$. The median MSD exponent [white circles in Fig. 4(d)] are all below 1, except at $\chi = 1$. Additionally, heightened mechanical heterogeneity leads to enhanced superdiffusive dynamics as there is a marked increase in median MSD exponent at $\chi = 1$ ($\alpha > 1$). For $\chi < 0.5$, no clear trend in MSD exponent is visible in Fig. 4(d) even though the max MSD increases in the same range. Despite the fact that the MSD exponents are characterized by a wide scatter, we observe that enhanced spatial mechanical heterogeneity led to heightened MSD values and MSD exponent.

IV. INDIVIDUAL CELL SOFTENING REGULATES CELL COLLECTIVE GROWTH RATE

The cell softening probability clearly determines the cell dynamics as evident from the MSD dependence on χ (discussed above). We next sought to evaluate whether cell softening impacts the volumetric growth of tumor cell collectives. Finding the biophysical underpinnings of tumor growth is of much interest. This is an important problem because accurate tumor growth modeling can be crucial in evaluating patient screening strategies [44], establishing radiation treatment protocols [45] as well as assist treatment decisions [46]. To answer this question, we quantified the 3D spatial spread of the cell collective using radius of gyration squared,

$$R_g^2(t) = \left\langle \frac{1}{N} \Sigma_{i=1}^{N} [\mathbf{r}_i(t) - \mathbf{R}_{CM}(t)]^2 \right\rangle. \tag{10}$$

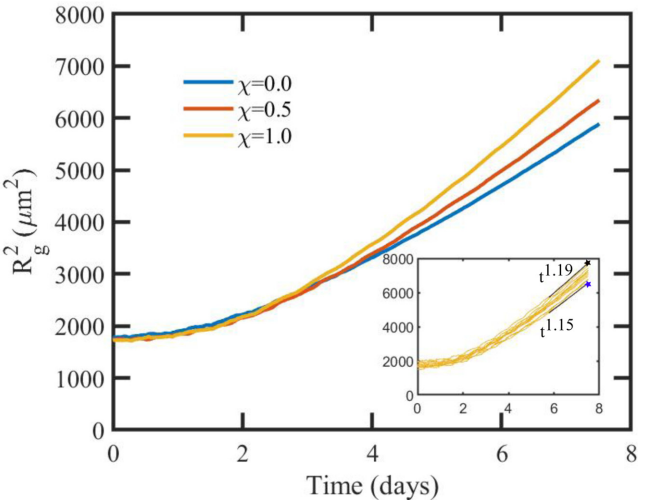

FIG. 5. Cell softening after division control cell collective growth. (a) Quantification of the ensemble-averaged (over 12 simulation runs) radius of gyration squared (R_g^2) of the 3D tumor cell collective over 7.5 days at $\chi = 0$, 0.5 and 1. Inset: R_g^2 from averaging over cells from individual simulation runs at $\chi = 1$. Maximum (max) R_g^2 values for two individual simulation runs are marked with stars. The time regime where R_g^2 is fit to power law in order to extract the exponent (β) is shown.

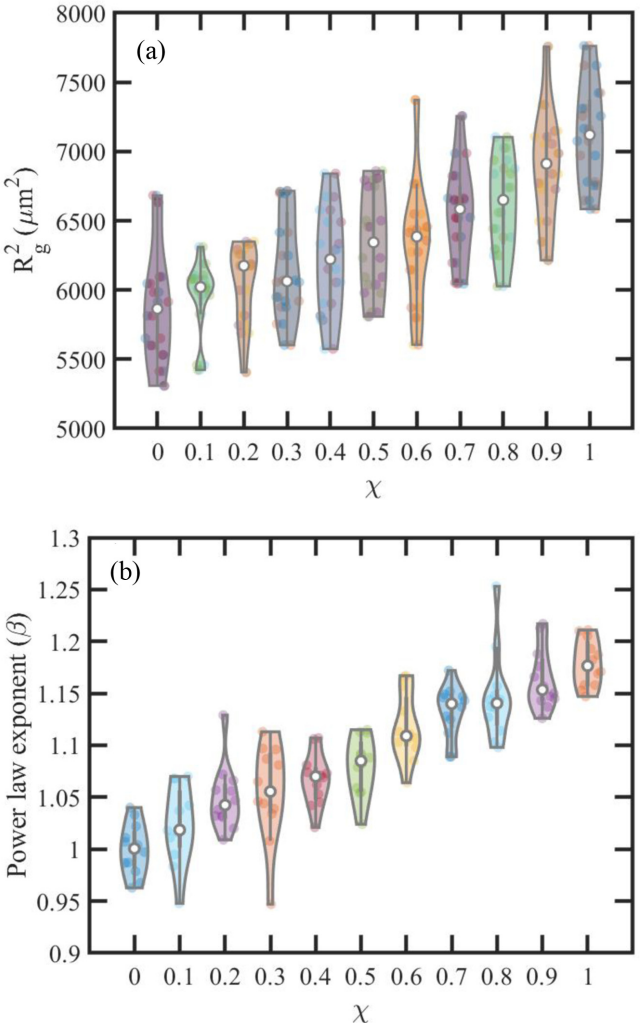

FIG. 6. Cell softening after division control cell collective growth. (a) Max value of R_g^2 at the end of simulation run at $t = 7.5$ days indicates significantly enhanced growth of tumor cell collective with increased probability of individual cells to soften (compare $\chi = 1$ to $\chi = 0$). Max R_g^2 value from each of the 12 simulations after averaging over individual cell R_g^2 is shown as colored dots. White dots are the median values, and the thick line within the violin distribution represent the interquartile range between the first and third quartiles. The bottom and top edges of thinner gray lines mark the lower and upper adjacent values respectively. (b) By fitting the average R_g^2 in each of the 12 simulation runs, we extracted the R_g^2 exponent β as a function of χ. Volumetric growth of the 3D cell collective is significantly enhanced at $\chi = 1$ as compared to $\chi = 0$.

The bracket $\langle \cdots \rangle$ denotes ensemble average over 12 different simulation runs at each value of χ for different initial conditions (see Appendix A). The average squared distance of all the cells from the center of mass gives a sense of the size of the 3D cell collective. Small R_g^2 values indicate cell positions that are localized in close proximity to the center of mass. In contrast, cells spatially distributed farther away from the center of mass leads to significantly larger R_g^2 values [47,48]. As a result, $R_g^2(t)$ as a function of time is a readout of the 3D cell collective volumetric growth. The time varying R_g^2 in Fig. 5 shows slow change at $t <\sim 3$ days followed by faster growth at $t > 4$ days. The R_g^2 values are indistinguishable between χ values at time below 4 days as compared to later times when R_g^2 is significantly larger for $\chi = 1$. Time-dependent scaling of R_g^2 based on a fit to power law $R_g^2(t) \sim t^\beta$ reveals important features of cell spatial distribution dynamics in 3D [49,50] (see inset of Fig. 5). When $\beta = 1$, cells exhibit diffusive random spread compared to when cells undergo directed spreading at $\beta > 1$. In contrast, restricted cell spreading leads to sublinear rise in R_g^2 with $\beta < 1$. The maximum (max) R_g^2 values (marked as stars in inset of Fig. 5) show a clear linear trend with χ [see Fig. 6(a)]. This implies that enhanced mechanical heterogeneity leads to significantly more spread out morphology of the 3D cell collective. The median value of max R_g^2 at $\chi = 0.1$ is $\sim$5800 μm^2 as compared to $\sim$7100 μm^2 at $\chi = 1$ as shown in Fig. 6(a).

Our results therefore indicate that heightened spatial mechanical heterogeneity leads to enhanced volumetric growth of the 3D cell collective with time-dependent spatial expansion of the cell collective being restricted when individual cells are stiffer. In contrast, cell softening favored faster expansion of the cell collective into the surrounding viscous medium with a median value of $\beta \sim 1.2$ [Fig. 6(b)]. Our results provide evidence into how spatial mechanical heterogeneity determines the spatial spread of 3D cell collectives. Hence, spatial mechanical heterogeneity consisting of a stiffer core cells and softer peripheral cells could aid more efficient volumetric growth of cell collectives.

V. CONCLUSION

How individual cell level mechanical changes impact cell dynamics and tumor growth is critical to understanding cancer

progression. In this respect, we studied how time-varying individual cell stiffness drives spatial mechanical heterogeneity in multicellular collectives by incorporating stiffening of cells immediately prior to division and softening after division into our minimal 3D tumor growth model. The probability for cells to soften after division is implemented in our model through the parameter χ which tunes actin rearrangement from the cell cortex into the cytoplasm. Hence, $\chi = 0.1$ implies a very low probability for cells to soften, while $\chi = 1$ implies a high probability for cells to soften after division. Our simulations show that cell division associated softening drives the emergence of spatial mechanical heterogeneity between the core and periphery of multicellular spheroids. The resulting spatial stiffness pattern consisting of a core made up of stiffer cells and peripheral softer cells enhances the 3D collective cell dynamics and volumetric growth of multicellular spheroids. Broadly, our computational results are consistent with experimental observations of spatial mechanical heterogeneity in 3D tumor organoids [18] and the heightened ability of softer tumor cells to metastasize [4,51]. As polymerization and depolymerization of the actomyosin network in the cell cortex lead to time-varying stiffening and softening of the cell, we show that such temporal stiffness variation at the single-cell level is essential in the emergence of mechanical heterogeneity at the scale of cell collectives. In addition to the increased space that cells explore in 3D cell collectives due to periodic stiffening and softening, our study shows that increased spatial mechanical heterogeneity is correlated with enhanced 3D spheroid growth. Our results therefore have important implications into understanding how time variations in single-cell mechanical properties determine the spatial organization and dynamics at the cell collective scale.

The presented model is sensitive to the cutoff radius at which cell stiffening occurs with important consequences on the spatial mechanical heterogeneity. The spatial mechanical heterogeneity is lost when cell stiffening occurs at a lower cutoff radius. On the hand, cell stiffening close to division events preserve mechanical heterogeneity (see Appendix D for further details). In terms of future work, we aim to build on these computational studies to implement analytical approaches to better understand the impact of nonequilibrium active matter cell properties on cell dynamics and spatial organization.

ACKNOWLEDGMENTS

A.M.K acknowledges funding from startup grants. A.M.K and T.D. acknowledge funding support from the Augusta University CURS Summer Scholars Program. T.D. acknowledges the hospitality of KITP at UC–Santa Barbara. A part of this research was completed at KITP and was supported in part by the NSF under Grant No. PHY-1748958. G.Z. acknowledges conversations and assistance from Dr. Nathan Yanasak regarding code speed up. The authors acknowledge the support of the Augusta University High Performance Computing Services (AUHPCS) for providing computational resources contributing to the results presented in this publication. We thank S. Sinha, X. Li, and D. Thirumalai for valuable comments on the manuscript.

APPENDIX A: INITIAL CONDITIONS

We initiated the simulations by placing 100 cells whose x, y, z coordinates are chosen from a normal distribution with zero mean and standard deviation 40 μm. In the present study, all the individual cell parameters are fixed except single-cell stiffness E_i which is varied within a physiological cell stiffness range. The initial cell sizes are assigned from a Gaussian distribution with a mean radius of 4.5 μm and standard deviation of 0.5 μm. As cells grow and divide, cell sizes vary in time. The simulated dense 3D cell aggregate was evolved for 650 000 s or 12τ. At each χ value, 12 different simulation runs allow for random initial positions of cells. Hence, our reported results account for varying initial conditions. Relevant simulation parameters are shown in Table I. The time-dependent coordinates of particles were recorded to calculate the dynamical observables relevant to this study.

APPENDIX B: SIMULATION MOVIES

Movies generated from the simulated 3D cell collective are available with their descriptions given below. The total duration of the movie is 650 000 s or $\approx 12\tau$. The time interval between consecutive frames is 1000 s.

Movie 1: 3D cell collective simulated at $\chi = 1$. Color bar indicates the stiffness of cells with dark blue indicating stiffer cells at 3 kPa. Softer cells are show in yellow color at 0.5 kPa. The observation frame is rotated to allow for a full 3D view of the tumor cell collective. The box is for 3D visualization purposes only [52].

Movie 2: Cross-sectional view of a 3D cell collective simulated at $\chi = 1$. Color bar indicates the stiffness of cells with dark blue indicating stiffer cells at 3 kPa. Softer cells are shown in yellow at 0.5 kPa. A view of a fixed 2D plane cutting through the 3D cell collective is shown [53].

APPENDIX C: GRADUAL INCREASE IN CELL STIFFNESS

In the spirit of a minimal computational model we consider a simplified form of cell stiffening and softening associated with cell division. Specifically, we consider cell stiffening and softening to be instantaneous while experimental reports point to a time interval of 20 min. We conducted further simulations to check the robustness of our modeling approach where the cell stiffening prior to division occurs gradually over a finite time interval of ∼20 min. To summarize, our primary conclusions pertaining to average cell stiffness vs time [Fig. 7(a)], spatial mechanical heterogeneity [Fig. 7(b)], cell dynamics [Fig. 7(c)], and spheroid growth [Fig. 7(d)] are robust as compared to when we considered the simplified case of instantaneous cell stiffening. Our key discovery of spatial mechanical heterogeneity with a stiffer core and softer cells in the periphery is observed even when the cells stiffen over a 20 min interval [see Fig. 7(b)]. Overall, the time-dependent stiffening process yield results that are consistent with our prior conclusions on average cell stiffness, spatial mechanical heterogeneity, cell dynamics, and growth of the cell collective.

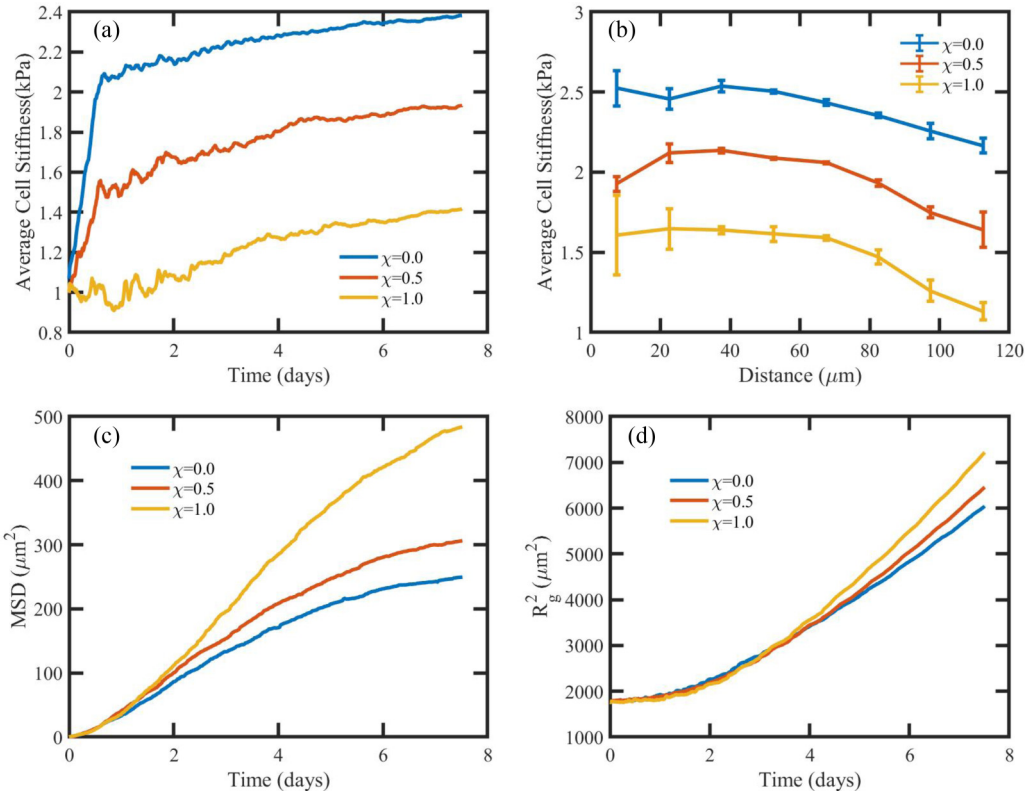

FIG. 7. Collective cell mechanical properties with finite time interval for cell stiffening. (a) Average cell stiffness of the entire cell collective as a function of time at three different values of $\chi = 0, 0.5, 1$ indicates a stiffening cell collective. Results are shown when cells stiffen over a finite time interval. $\chi = 0$ leads to a stiffer cell collective as compared to $\chi = 1$. (b) Average stiffness of cell subpopulations as a function of distance from the core with cell subpopulations categorized according to their distances from the center of mass of the 3D cell collective at $t = 12\tau_{\text{min}}$. Spatial mechanical heterogeneity with stiffer core and softer cells in the periphery is evident. Enhanced cell softening parameter ($\chi = 1$) leads to heightened mechanical heterogeneity. Mean values and the error bar as calculated from the standard deviation is indicated. (c) Ensemble-averaged MSD of cells vs time at three different values of χ. The data are averaged over three independent simulation runs by tracking ~200 cells over the complete simulation at each value of χ. (d) Ensemble-averaged (over three simulation runs) radius of gyration squared (R_g^2) of the 3D tumor cell collective over 7.5 days at $\chi = 0, 0.5, 1$. This quantifies the spatial size of the multicellular collective as a function of time.

APPENDIX D: VARYING CRITICAL CELL SIZE FOR THE ONSET OF CELL STIFFENING

We checked the sensitivity of our results to the cell size at which the stiffness is modulated. We anticipate that the cutoff radius at which cell stiffness is increased will have a significant impact on our results as we discuss here. If stiffness is increased early on in the cell cycle corresponding to a lower cutoff radius, cells would remain stiffer for longer. On the other hand, a larger cutoff radius implies that cells remain softer for longer. To test these predictions, we performed additional simulations varying the cutoff radius at which cell stiffness is increased prior to division. For the results in the main text, a cell grows in size and as it approaches the mitotic radius $[R_i(t = t^*)/R_m = 0.98]$, undergo stiffening. This was chosen so as to model the experimental scenario where cells start stiffening ~20 min prior to division. For the mean cell cycle time of $\tau = 54\,000$ s, the time interval between cell stiffening and reaching the mitotic R_m when a cell divides is given by $t_{\text{int}} \sim (1 - 0.98) \times 54\,000$ s ~ 20 min. We performed additional simulation at smaller $R_i(t = t^*)/R_m = 0.8$ (see left 3 panels in Fig. 8) and larger $R_i(t = t^*)/R_m = 0.995$ (see right three panels in Fig. 8) cutoff radii at which cells stiffen. The smaller cutoff radius corresponds to a longer time interval over which the cell remains stiff before division while the larger cutoff radius means that cells remain stiff for only a short interval before division. For the stiffening radius of $R_i(t = t^*)/R_m = 0.8$, the average time interval to division would be ≈180 min, while for $R_i(t = t^*)/R_m = 0.995$, the average time interval to division would be ≈4 min. Hence, it should be kept in mind that these different scenarios are an order of magnitude smaller and larger compared to experimental results reported for the time point at which cells stiffen before division. To summarize our results, varying cell softening probability led to no significant differences in cell dynamics [Fig. 8(a)], cell collective size [Fig. 8(b)] and mechanical heterogeneity [Fig. 8(c)] when cutoff radius is $(R_i(t = t^*)/R_m = 0.8)$. On the other hand, at higher cutoff radius of $[R_i(t = t^*)/R_m = 0.995]$, cell dynamics is enhanced [Fig. 8(d)], larger tumor size growth [Fig. 8(e)] and significant mechanical heterogeneity result [Fig. 8(f)] with higher probability for cell softening.

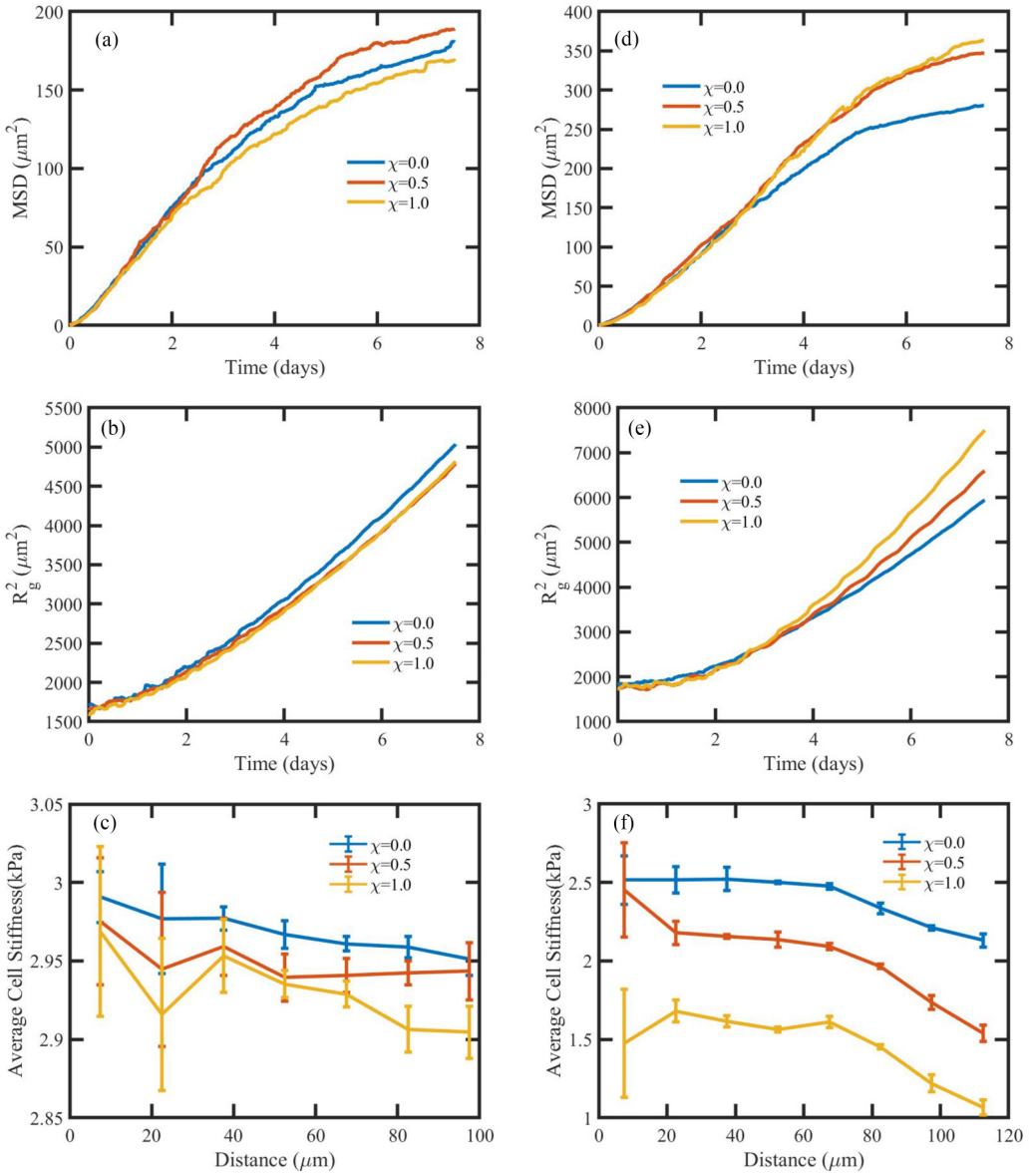

FIG. 8. Collective cell mechanical properties with varying radius cutoff for cell stiffening. Left panels (a)–(c) are for lower cutoff radius for cell stiffening ($R_i(t = t^*)/R_m = 0.8$). Right panels (d)–(f) are at higher cutoff radius for cell stiffening $R_i(t = t^*)/R_m = 0.995$. (a) Ensemble-averaged MSD of cells vs time at three different values of χ at lower cutoff radius of $[R_i(t = t^*)/R_m = 0.8]$. The data are averaged over three independent simulation runs by tracking ∼200 cells over the complete simulation at each value of χ. Cell dynamics is not correlated with higher probability to soften. (b) Ensemble-averaged (over three simulation runs) radius of gyration squared (R_g^2) of the 3D tumor cell collective over 7.5 days at $\chi = 0, 0.5, 1$. This quantifies the spatial size of the multicellular collective as a function of time. No clear difference in tumor cell collective size is observed due to changes in χ. (c) Average stiffness of cell subpopulations as a function of distance from the core with subpopulations categorized according to their distances from the center of mass of the 3D cell collective at $t = 12\tau_{\min}$. Spatial mechanical heterogeneity with stiffer core and softer cells in the periphery is not observed irrespective of varying the cell softening parameter (χ). (d) Ensemble-averaged MSD of cells vs time at three different values of χ at higher cutoff radius of $[R_i(t = t^*)/R_m = 0.995]$. Higher probability for cell softening leads to enhanced cell dynamics. (e) Radius of gyration squared (R_g^2) indicates that tumor cell collective is larger at $\chi = 1$ compared to $\chi = 0$. (f) Spatial mechanical heterogeneity with stiffer core and softer cells in the periphery is observed at higher cutoff radius for cell stiffening.

[1] C. T. Mierke, The fundamental role of mechanical properties in the progression of cancer disease and inflammation, Rep. Prog. Phys. **77**, 076602 (2014).

[2] J. Lv, Y. Liu, F. Cheng, J. Li, Y. Zhou, T. Zhang, N. Zhou, C. Li, Z. Wang, L. Ma *et al.*, Cell softness regulates tumorigenicity and stemness of cancer cells, EMBO J. **40**, e106123 (2021).

[3] P.-H. Wu, D. R.-B. Aroush, A. Asnacios, W.-C. Chen, M. E. Dokukin, B. L. Doss, P. Durand-Smet, A. Ekpenyong, J. Guck, N. V. Guz *et al.*, A comparison of methods to assess cell mechanical properties, Nat. Methods **15**, 491 (2018).

[4] V. Swaminathan, K. Mythreye, E. T. O'Brien, A. Berchuck, G. C. Blobe, and R. Superfine, Mechanical stiffness grades

metastatic potential in patient tumor cells and in cancer cell lines, Cancer Res. **71**, 5075 (2011).

[5] S. E. Cross, Y.-S. Jin, J. Rao, and J. K. Gimzewski, Nanomechanical analysis of cells from cancer patients, Nat. Nanotechnol. **2**, 780 (2007).

[6] S. Hurst, B. E. Vos, M. Brandt, and T. Betz, Intracellular softening and increased viscoelastic fluidity during division, Nat. Phys. **17**, 1270 (2021).

[7] S. Nam and O. Chaudhuri, Mitotic cells generate protrusive extracellular forces to divide in three-dimensional microenvironments, Nat. Phys. **14**, 621 (2018).

[8] A. V. Taubenberger, B. Baum, and H. K. Matthews, The mechanics of mitotic cell rounding, Front. Cell Dev. Biol. **8**, 687 (2020).

[9] M. P. Stewart, J. Helenius, Y. Toyoda, S. P. Ramanathan, D. J. Muller, and A. A. Hyman, Hydrostatic pressure and the actomyosin cortex drive mitotic cell rounding, Nature (London) **469**, 226 (2011).

[10] E. Fischer-Friedrich, Y. Toyoda, C. J. Cattin, D. J. Müller, A. A. Hyman, and F. Jülicher, Rheology of the active cell cortex in mitosis, Biophys. J. **111**, 589 (2016).

[11] P. Chugh and E. K. Paluch, The actin cortex at a glance, J. Cell Sci. **131**, jcs186254 (2018).

[12] G. Salbreux, G. Charras, and E. Paluch, Actin cortex mechanics and cellular morphogenesis, Trends Cell Biol. **22**, 536 (2012).

[13] J. Howard, *Mechanics of Motor Proteins and the Cytoskeleton* (Sinauer Associates, Sunderland, MA, 2001).

[14] M. P. Stewart, Y. Toyoda, A. A. Hyman, and D. J. Muller, Force probing cell shape changes to molecular resolution, Trends Biochem. Sci. **36**, 444 (2011).

[15] Y. Fujii, W. C. Koizumi, T. Imai, M. Yokobori, T. Matsuo, K. Oka, K. Hotta, and T. Okajima, Spatiotemporal dynamics of single cell stiffness in the early developing ascidian chordate embryo, Commun. Biol. **4**, 341 (2021).

[16] C. Rianna, M. Radmacher, and S. Kumar, Direct evidence that tumor cells soften when navigating confined spaces, Mol. Biol. Cell **31**, 1726 (2020).

[17] C. L. Marchant, A. N. Malmi-Kakkada, J. A. Espina, and E. H. Barriga, Cell clusters softening triggers collective cell migration in vivo, Nat. Mater. **21**, 1314 (2022).

[18] Y. L. Han, A. F. Pegoraro, H. Li, K. Li, Y. Yuan, G. Xu, Z. Gu, J. Sun, Y. Hao, S. K. Gupta *et al.*, Cell swelling, softening and invasion in a three-dimensional breast cancer model, Nat. Phys. **16**, 101 (2020).

[19] D. Drasdo and S. Höhme, A single-cell-based model of tumor growth in vitro: Monolayers and spheroids, Phys. Biol. **2**, 133 (2005).

[20] G. Schaller and M. Meyer-Hermann, Multicellular tumor spheroid in an off-lattice Voronoi-Delaunay cell model, Phys. Rev. E **71**, 051910 (2005).

[21] A. N. Malmi-Kakkada, X. Li, H. S. Samanta, S. Sinha, and D. Thirumalai, Cell Growth Rate Dictates the Onset of Glass to Fluidlike Transition and Long Time Superdiffusion in an Evolving Cell Colony, Phys. Rev. X **8**, 021025 (2018).

[22] A. N. Malmi-Kakkada, S. Sinha, X. Li, and D. Thirumalai, Adhesion strength between cells regulate nonmonotonic growth by a biomechanical feedback mechanism, Biophys. J. **121**, 3719 (2022).

[23] S. Sinha, A. N. Malmi-Kakkada, X. Li, H. S. Samanta, and D. Thirumalai, Spatially heterogeneous dynamics of cells in a growing tumor spheroid: Comparison between theory and experiments, Soft Matter **16**, 5294 (2020).

[24] S. Sinha and D. Thirumalai, Self-generated persistent random forces drive phase separation in growing tumors, J. Chem. Phys. **153**, 201101 (2020).

[25] S. Sinha and A. N. Malmi-Kakkada, Inter-particle adhesion regulates the surface roughness of growing dense three-dimensional active particle aggregates, J. Phys. Chem. B **125**, 10445 (2021).

[26] D. K. Schlüter, I. Ramis-Conde, and M. A. Chaplain, Multi-scale modelling of the dynamics of cell colonies: Insights into cell-adhesion forces and cancer invasion from in silico simulations, J. R. Soc. Interface **12**, 20141080 (2015).

[27] T. E. Gorochowski, Agent-based modelling in synthetic biology, Essays Biochem. **60**, 325 (2016).

[28] M. Sherar, M. Noss, and F. Foster, Ultrasound backscatter microscopy images the internal structure of living tumour spheroids, Nature (London) **330**, 493 (1987).

[29] J. J. Casciari, S. V. Sotirchos, and R. M. Sutherland, Variations in tumor cell growth rates and metabolism with oxygen concentration, glucose concentration, and extracellular ph, J. Cell. Physiol. **151**, 386 (1992).

[30] M. Plodinec, M. Loparic, C. A. Monnier, E. C. Obermann, R. Zanetti-Dallenbach, P. Oertle, J. T. Hyotyla, U. Aebi, M. Bentires-Alj, R. Y. Lim *et al.*, The nanomechanical signature of breast cancer, Nat. Nanotechnol. **7**, 757 (2012).

[31] J. Irianto, C. R. Pfeifer, Y. Xia, and D. E. Discher, Snapshot: Mechanosensing matrix, Cell **165**, 1820 (2016).

[32] S. P. Ramanathan, J. Helenius, M. P. Stewart, C. J. Cattin, A. A. Hyman, and D. J. Muller, Cdk1-dependent mitotic enrichment of cortical myosin II promotes cell rounding against confinement, Nat. Cell. Biol. **17**, 148 (2015).

[33] M. Kelkar, P. Bohec, and G. Charras, Mechanics of the cellular actin cortex: From signalling to shape change, Curr. Opin. Cell Biol. **66**, 69 (2020).

[34] E. M. Purcell, Life at low Reynolds number, Am. J. Phys. **45**, 3 (1977).

[35] S. Sinha, X. Li, R. Das, and D. Thirumalai, Mechanical feedback controls the emergence of dynamical memory in growing tissue monolayers, J. Chem. Phys. **156**, 245101 (2022).

[36] Y. Shen, B. S. Schmidt, H. Kubitschke, E. W. Morawetz, B. Wolf, J. A. Käs, and W. Losert, Detecting heterogeneity in and between breast cancer cell lines, Cancer Converg. **4**, 1 (2020).

[37] J. Guck, S. Schinkinger, B. Lincoln, F. Wottawah, S. Ebert, M. Romeyke, D. Lenz, H. M. Erickson, R. Ananthakrishnan, D. Mitchell *et al.*, Optical deformability as an inherent cell marker for testing malignant transformation and metastatic competence, Biophys. J. **88**, 3689 (2005).

[38] W. Xu, R. Mezencev, B. Kim, L. Wang, J. McDonald, and T. Sulchek, Cell stiffness is a biomarker of the metastatic potential of ovarian cancer cells, PLoS One. **7**, e46609 (2012).

[39] A. Fritsch, M. Höckel, T. Kiessling, K. D. Nnetu, F. Wetzel, M. Zink, and J. A. Käs, Are biomechanical changes necessary for tumour progression? Nat. Phys. **6**, 730 (2010).

[40] C. Alibert, B. Goud, and J.-B. Manneville, Are cancer cells really softer than normal cells? Biol. Cell **109**, 167 (2017).

[41] J. Ranft, M. Basan, J. Elgeti, J.-F. Joanny, J. Prost, and F. Jülicher, Fluidization of tissues by cell division and apoptosis, Proc. Natl. Acad. Sci. USA **107**, 20863 (2010).

[42] D. Matoz-Fernandez, K. Martens, R. Sknepnek, J. Barrat, and S. Henkes, Cell division and death inhibit glassy behaviour of confluent tissues, Soft Matter **13**, 3205 (2017).

[43] C. P. Brangwynne, G. H. Koenderink, F. C. MacKintosh, and D. A. Weitz, Intracellular transport by active diffusion, Trends Cell Biol. **19**, 423 (2009).

[44] A. Talkington and R. Durrett, Estimating tumor growth rates in vivo, Bull. Math. Biol. **77**, 1934 (2015).

[45] P. Castorina, T. Deisboeck, P. Gabriele, and C. Guiot, Growth laws in cancer: Implications for radiotherapy, Radiat. Res. **168**, 349 (2007).

[46] E. Comen, P. G. Morris, and L. Norton, Translating mathematical modeling of tumor growth patterns into novel therapeutic approaches for breast cancer, J. Mammary Gland Biol. Neoplasia **17**, 241 (2012).

[47] M. J. Saxton, Lateral diffusion in an archipelago. Single-particle diffusion, Biophys. J. **64**, 1766 (1993).

[48] J. Roy, J. Mazzaferri, J. G. Filep, and S. Costantino, A haptotaxis assay for neutrophils using optical patterning and a high-content approach, Sci. Rep. **7**, 2869 (2017).

[49] B. R. Parry, I. V. Surovtsev, M. T. Cabeen, C. S. O'Hern, E. R. Dufresne, and C. Jacobs-Wagner, The bacterial cytoplasm has glass-like properties and is fluidized by metabolic activity, Cell **156**, 183 (2014).

[50] M. C. Gonzalez, C. A. Hidalgo, and A.-L. Barabasi, Understanding individual human mobility patterns, Nature (London) **453**, 779 (2008).

[51] V. Panzetta, I. Musella, I. Rapa, M. Volante, P. A. Netti, and S. Fusco, Mechanical phenotyping of cells and extracellular matrix as grade and stage markers of lung tumor tissues, Acta Biomater. **57**, 334 (2017).

[52] https://augustauniversity.box.com/s/zyse7otymd2uu2zt451vgx6g3x28abwa.

[53] https://augustauniversity.box.com/s/xxa0eezs2rae2yj7shlp7kyk7dvx19m0.